Available online at www.sciencedirect.com
SCIENCE DIRECT®
Journal of Solid State Chemistry 179 (2006) 270–277
JOURNAL OF SOLID STATE CHEMISTRY
www.elsevier.com/locate/jssc

Nitrogen-doped zirconia: A comparison with cation stabilized zirconia

Jong-Sook Lee[a,*], Martin Lerch[b], Joachim Maier[a]

[a]*Max-Planck-Institut für Festkörperforschung, 70569 Stuttgart, Germany*
[b]*Technische Universität Berlin, 10623 Berlin, Germany*

Received 25 July 2005; received in revised form 28 September 2005; accepted 2 October 2005
Available online 17 November 2005

Abstract

The conductivity behavior of nitrogen-doped zirconia is compared with that of zirconia doped with lower-valent cations and discussed in the framework of defect–defect interactions. While nominally introducing the same number of vacancies as yttrium, nitrogen dopants introduced in the anion sublattice of zirconia lead to substantially different defect kinetics and energetics. Compared to the equivalent yttrium doping nitrogen doping in the Y–Zr–O–N system substantially increases the activation energy and correspondingly decreases the conductivity at temperatures below 500 °C in the vacancy range below 4 mol%. The comparison of N-doped zirconia and zirconia systems doped with size-matched cation stabilizers, such as Sc, Yb and Y, shows that elastically driven vacancy–vacancy ordering interactions can phenomenologically account for the temperature- and composition-dependence. It is striking that materials with superior high-temperature conductivities due to weak dopant–vacancy interactions undergo severe deterioration at low temperature due to the strong vacancy-ordering. The analysis also explains qualitatively similar effects of Y co-doping in Yb-, Sc-, and N-doped zirconia. Small amount of Y in N-doped zirconia as well as in Sc-doped zirconia appears to hinder the formation of the long-range ordered phase and thus enhance the conductivity substantially.

Keywords: Zirconia; Nitrogen; Conductivity; Vacancy ordering; Elastic defect interaction

1. Introduction

When dissolved in the zirconia matrix aliovalent anions such as nitrogen introduce oxygen vacancies similarly as well-known cation dopants Y, Ca, Sc, etc., and 'stabilize' zirconia in the tetragonal or cubic phase, in which the vacancy distribution is grossly random. Within the last decade N-containing zirconia has been drawing renewed attention [1–5] while prior studies date back to the sixties [6–9]. Most notable in recent studies was the finding that in the presence of a small amount of Y (2 or 3 mol% Y_2O_3) N successfully stabilizes zirconia in tetragonal and cubic phases even at low temperatures [1,2,4,5,10,11], while N-doping alone results in the formation of ordered-vacancy phases in rhombohedral or primitive trigonal structures below 1000 °C [12,13].

While N- and Y-incorporation generate identical numbers of vacancies according to

$$Y_2O_3 + 2Zr_{Zr}^{\times} + O_O^{\times} \rightarrow 2Y'_{Zr} + V_O^{\cdot\cdot} + 2ZrO_2;$$
$$N_2 + 3O_O^{\times} \rightarrow 2N'_O + V_O^{\cdot\cdot} + \tfrac{3}{2}O_2, \quad (1)$$

dopant ions in anion sublattice N'_O and cation sublattice Y'_{Zr} are expected to lead to substantially different consequences in defect thermodynamics and kinetics. One point is that fluorite structure offers a much higher diffusivity for the nitride ion (N^{3-}) than for the cation stabilizers [4,14]. In addition, interactions between N^{3-} and the other anion species (O^{2-}, $V_O^{\cdot\cdot}$) and between N^{3-} and cationic species (Zr^{4+}, Y^{3+}) should be taken account of. Structural investigations in Y–Zr–O–N system have not been reported until recently [15,16] and further progress is still awaited to atomistically explain the conductivity effects discussed in this work.

In the present contribution the N effects on the conductivity of zirconia will be revisited based on recent results of the authors [17–19]. In view of lack of detailed

*Corresponding author. Fax: +49 711 689-1722.
E-mail address: jong-sook.lee@fkf.mpg.de (J.-S. Lee).

0022-4596/$ - see front matter © 2005 Elsevier Inc. All rights reserved.
doi:10.1016/j.jssc.2005.10.012

structural and modelling work, we attempt to understand the behavior phenomenologically by comparison with the effects of conventional cation stabilizers. Surprisingly, even for much discussed cation-stabilized zirconia solid solutions, despite decades of studies, the description of the nature of defect interactions seems conflicting and confusing. Only recently some significant progress was achieved [20–24].

2. Defect interactions in Zirconia

Zirconia-based solid electrolytes involve a large number of vacancies ($\gg 1$ mol%) and unsurprisingly the transport characteristics have been considered in terms of defect interactions. Dopant–vacancy interactions resulting in associates and clusters as a consequence of electrostatic attraction between point charges are the most commonly employed explanation accounting for (i) an increased low-temperature activation energy as observed for Y- or Sc-doped zirconia and (ii) an increased activation energy and a decrease conductivity at high dopant levels as observed in all cases. Moreover, the inferior conductivity of $CaO-ZrO_2$ system with divalent dopants (of effective charge -2), when compared to $Y_2O_3-ZrO_2$ with trivalent dopants (of effective charge -1), has been ascribed to the stronger Coulombic interaction [25,26].

On the other hand, the conductivity variation with the dopant size among different trivalent dopants of Y, Yb and Sc suggested the importance of elastic interaction [27,28], which is also supported by recent theoretical calculations [20–22,29,30]. The 'size-matched' or slightly larger Sc dopant has the least dopant–vacancy interaction and thus leads to the so far highest ionic conductivity among zirconia-based solid electrolytes, followed by the oversized Yb and Y dopants. Moreover, the finding that oversized Y and Ca ions avoid the nearest-neighboring sites to the vacancies [23,31–34] cannot be explained by simple electrostatic (attractive) interactions between dopants and vacancies.

The elastic origin of the defect interactions can be described by the lattice relaxations induced by an anion vacancy in the crystal structure of zirconia. As shown in Fig. 1 six neighboring oxygen ions are pulled towards a vacancy along [1 0 0] direction (and the four neighboring cations are pushed out along [1 1 1] direction), in fact, driven by the electrostatics. These displacements of ions have been evidenced theoretically [20,29,30] as well as indicated in experimental studies [23,35–37]. The lattice relaxation is not limited to the nearest neighborhood of a vacancy but is of long range [20,23,29]. The repulsive interactions between vacancies and oversized dopants arise since the oversized dopants as nearest neighbors to the vacancies (as indicated in Fig. 1) hinder the relaxation of the oxygen lattice.

Less intelligible may be the ordering of vacancies along [1 1 1] direction [23,30,35,36]. Recent theoretical calculations [21,22] suggested that in Y- or Sc-doped zirconia 'elastically' attractive vacancy–vacancy interactions favoring a vacancy ordering (in spite of the Coulombic repulsion) are even stronger than 'elastically' repulsive dopant–vacancy interaction. This has been related to the formation of $Zr_3M_4O_{12}$ ($M = Y, Sc$) with [1 1 1] vacancy pairs (as indicated in Fig. 1) in short-range or in long-range. The energetic preference of vacancy pairs, even when the vacancies can be further apart on purely electrostatic grounds, is described as an attractive delocalized elastic interaction [22]. In Y- or Sc-doped system the electrostatic interactions of simple point-charge electrostatics are shown to be essentially similar to the complex quantum-mechanical 'electronic' interactions of the 'unrelaxed' lattice, indicating little influence of electronic parameters like polarizability, electronegativity, etc. [22].

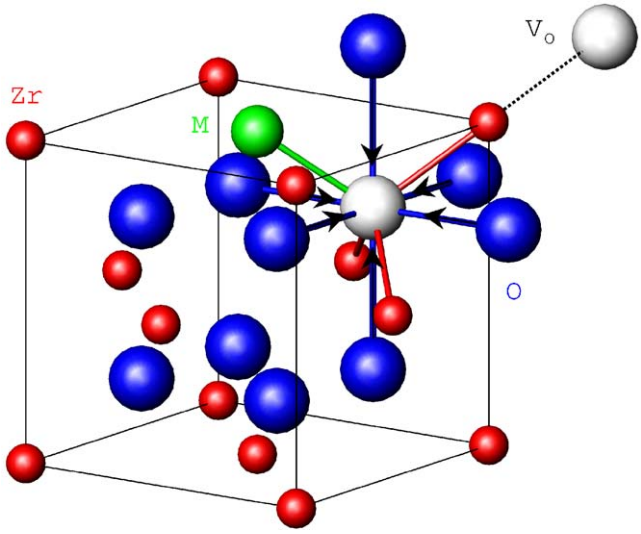

Fig. 1. Fluorite structure indicating displacements of six neighboring oxygen ions in [1 0 0] direction around an oxygen vacancy (V_O), one oversized dopant ion (M) neighboring a vacancy, and a [1 1 1] vacancy pair.

Vacancy ordered structures consisting of so-called Bevan clusters or [1 1 1] vacancy pairs, as observed in Y- or Sc-doped zirconia, are the pronounced feature in nitrogen-containing zirconia [3,7,13,38]. The β-type phases (β, β', β'', etc.) in nitrogen-doped zirconia can be described as arrangements of Bevan clusters containing [1 1 1] vacancy pair and perfect fluorite unit [7,9,13,38–40]. An indication of N/O ordering was also found in the β'-phase in the Mg–Zr–O–N system [41]. A recent study [15] revealed large regions of tetragonal long-range order in a Y–Zr–O–N single crystal sample with a total vacancy concentration of ~6 mol% (of which 1.1 mol% stem from Y-doping), which conversely indicates concentrated vacancies in the cubic region of the crystal due to a stronger vacancy-ordering interaction resulting from N-doping. The detailed impact of the N polarizablity and the covalency of the Zr–N bond is yet to be clarified.

3. Conductivity behavior of Y–Zr–O–N system

Fig. 2 shows the bulk conductivity of Y–Zr–O–N ceramics obtained by impedance spectroscopy [17–19].

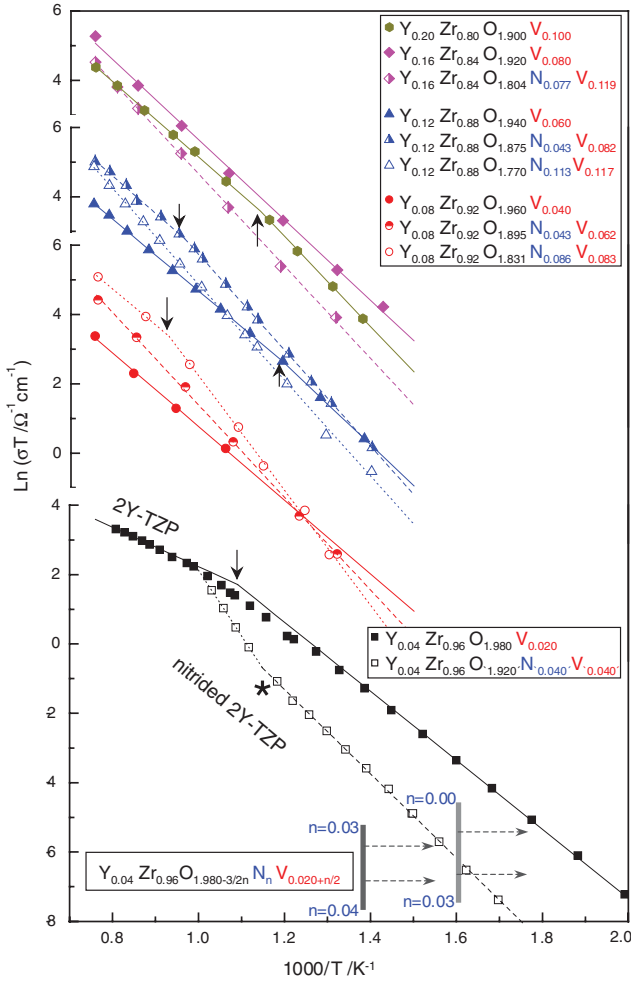

Fig. 2. Temperature dependence of conductivity of Y–Zr–O–N materials.

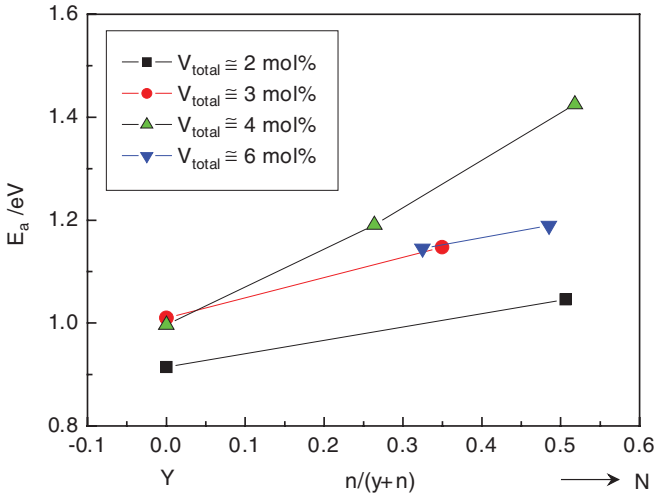

Fig. 3. Activation energy values (of the low-temperature regimes) as a function of nitrogen contribution ($n/(y+n)$) in the Y–N binary system for the total vacancy concentrations of 2, 3, 4, and 6 mol%.

The samples for the upper three groups of graphs (each with three plots) were obtained by direct nitridation of the oxides (Y–Zr–O), which had been prepared by a solution–precipitation method. The details of the sample preparation can be found in Ref. [18]. The sample composition can be formulated as $Y_yZr_{1-y}O_{2-y/2-3n/2}N_n$ with the total vacancy concentrations (V_{total}) being $(y+n)/4 \times 100$ mol% according to Eq. (1).

Bottom plots in Fig. 2 represent the data of a 2Y-TZP specimen ($Y_{0.04}Zr_{0.96}O_{1.98}V_{0.02}$) prepared from commercial powder (TZ-2Y, Tosoh, Japan) (in solid squares) and nitrided 2Y-TZP (in open squares) [17]. The N content of the nitrided 2Y-TZP specimen is a rough estimate in reference to similarly prepared specimens [19]. The two lines at the bottom represent the conductivity variation of the N-graded specimens measured by microcontact impedance spectroscopy [19]. The N stoichiometry (n) varies from 0 to ~0.03 ($T_{\text{set}} = 350\,^{\circ}\text{C}$) and from 0.03 and ~0.04 ($T_{\text{set}} = 450\,^{\circ}\text{C}$), respectively. The shift indicates from the T_{set} of the hot plate in the microcontact measurements to the supposed correct specimen temperatures based on the measurements using macro-sized electrodes.

In Fig. 2 Arrhenius fits are represented by lines. The arrows indicate two different temperatures regimes in which, as typically observed for Y- or Sc-doped zirconia, the activation energy at low-temperature regime is higher than that at high temperature. The nitrided 2Y-TZP specimen exhibits an opposite curvature (indicated by asterisk), i.e. a transition to a higher high-temperature slope around 600 °C, which may indicate a step-wise transition to a high-temperature regime as seen in strongly scandia-doped zirconia (>9 mol% Sc_2O_3). The measurement was however limited to ~700 °C. The effect of dopant concentrations and compositions on the activation energy is shown in Fig. 3 for the Y–N quasi-binary system. The activation energy values (of the low-temperature regime) are given for different total vacancy concentrations, i.e. $V_{\text{total}} = (y+n)/4 \times 100$ mol% and plotted as a function of nitrogen contribution. The results then reveal that the activation energy increases with V_{total} up to 4 mol% and, for given V_{total}, with the nitrogen fraction.

Fig. 4 displays conductivity isotherms corresponding to Fig. 2. The isotherms in solid symbols, separately displayed in Fig. 5(a), represent the dependence on the Y amount in purely Y-doped zirconia: the maximum conductivity is observed at around 4 mol% vacancies (or 8 mol% of Y_2O_3) with maximum becoming less pronounced with decreasing temperature. Figs. 5(b)–(d) show the effects of N addition to the zirconia ceramics already containing fixed Y amounts as 8, 6, and 4 mol% Y_2O_3, respectively. At 1043 °C all the isotherms almost coincide with each other but an enhanced conductivity in N-containing specimens, compared to those with Y only (in solid symbols), is indicated (see Fig. 4). The isotherms at 727 °C are the same regardless of dopant composition. Apparently N and Y behave identically. At lower temperatures (496 °C, 394 °C), however, N addition strongly decreases conductivity compared to the equivalent amount of Y, which is more

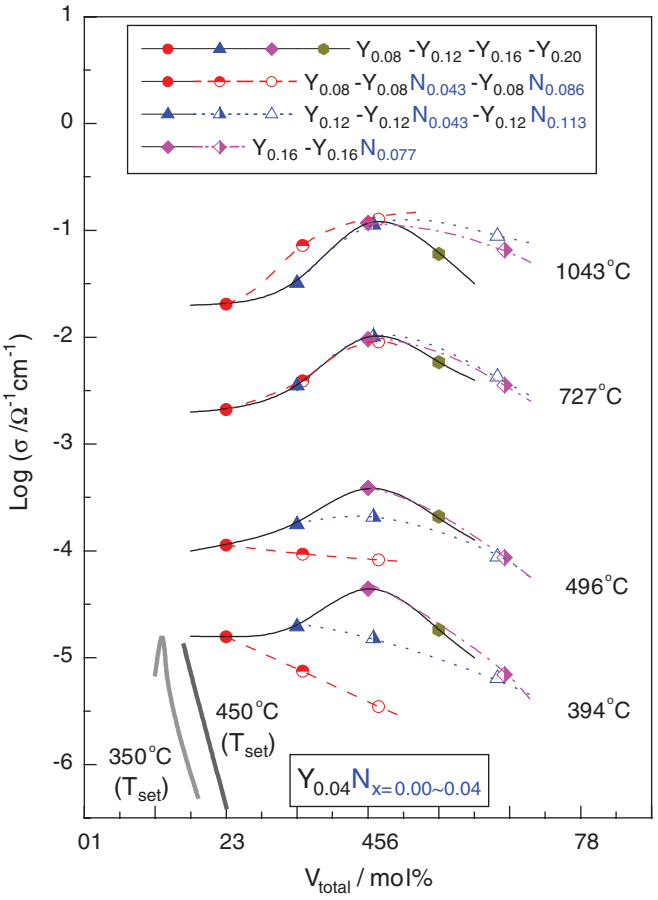

Fig. 4. Conductivity isotherms of Y–Zr–O–N materials as a function of the total vacancy concentrations. Filled symbols connected with solid lines represent conductivity dependence of zirconia doped with yttria only. Different symbols display the effect of nitrogen addition for the fixed concentrations of Y_2O_3, 4, 6 and 8 mol%. The respective plots are separately shown in Fig. 5. The two line graphs represent the effect of nitrogen addition in zirconia with 2 mol% yttria (2Y-TZP) measured by micro-contact impedance spectroscopy at $T_{set} = 350$ and 450 °C, and expanded in Fig. 6.

pronounced in the compositions with lower Y content. In the case of 4 mol% Y_2O_3, Fig. 5(d), the opposite effects of N addition at high temperature and at low temperature are clearly shown. The strong conductivity decrease with decreasing temperature in N-rich compositions is equivalently shown by their high activation energy values, e.g. 1.42 eV for $Y_{0.08}N_{0.086}$ composition (Fig. 3).

Two line graphs in the vacancy range between 1 and 2 mol% in Fig. 4, magnified in Fig. 6, represent the effect of N addition in zirconia containing 2 mol% Y_2O_3 (2Y-TZP). The isotherms are obtained from the conductivity profiles on the N-graded zirconia measured by microcontact impedance spectroscopy [19] and the nitrogen concentration profiles measured by Auger electron spectroscopy [4]. The growth of large-grained nitrided surface layers consisted of tetragonal dispersoids and cubic phase matrix (i.e. partially stabilized zirconia (PSZ)) into the sintered 2Y-TZP pellets followed a parabolic rate law driven by N flux [4]. In Fig. 6, the dotted region corresponds to the concentration step at the growth front bordering the TZP and PSZ region. While in the TZP region a slight variation with nitrogen concentration was indicated, a strong conductivity decrease with nitrogen concentration in the PSZ material was clearly observed. The extreme conductivity decrease with N addition is consistent with the tendency shown by the upper curves in Fig. 4 and can be attributed to the smaller Y content of the specimen and to the lower measurement temperatures. It should be noted that the present observation concerns the zirconia with low dopant levels between 1 and 4 mol% vacancies, while the conductivity decrease with dopant levels in Y-doped zirconia has been mainly referring to the high dopant concentrations beyond maximum conductivity composition of 4 mol% vacancies in the cubic phase region.

Fig. 7 represents the conductivity isotherms of the Y–N binary system for a constant total vacancy concentration of 4 mol% (cf. Fig. 5). While at high temperatures above 700 °C the conductivity does not depend much on the dopant compositions, it strongly decreases with increasing N contribution at low temperatures. The conductivity increase with N fraction expected at higher temperature is schematically represented by the T_{high} isotherm, while a lower temperature (T_{low}) isotherm represents a more drastic conductivity deterioration with increasing N fraction. Further aspects of Fig. 7 will be addressed in the next section.

4. Comparison with other zirconia systems

To understand the conduction mechanism in the Y–Zr–O–N materials described above, the situation in other zirconia systems with conventional cation stabilizers will be briefly examined. Fig. 8 represents schematically the temperature and dopant-concentration dependence of conductivity in $CaO-ZrO_2$ (a), $Y_2O_3-ZrO_2$ (b) and $Sc_2O_3-ZrO_2$ (c). The temperature dependence of three compositions ($C_1 < C_2 < C_3$) (left) and the concentration dependence at three temperatures ($T_1 < T_2 < T_3$) (right) are displayed.

The $CaO-ZrO_2$ system [42–46] exhibits an Arrhenius behavior over a wide temperature range from 300 °C up to ~1100 °C. Conductivity bends or stepwise transitions occur at about 1100 °C, which was attributed to an order–disorder transition [42,46]. Diffraction studies indicated a decrease of the diffuse scattering and an increase of the oxygen temperature factor around the transition temperature [47,48], but the nature of this transition seems not clarified yet. The maximum conductivity composition of ~13 mol% of CaO (13CSZ), which corresponds to the minimum amount of CaO necessary to stabilize the cubic phase (*c*), hardly changes with temperature and the maxima tend to be more pronounced with decreasing temperature. While the increasing activation energy at high dopant levels was attributed to the increasing

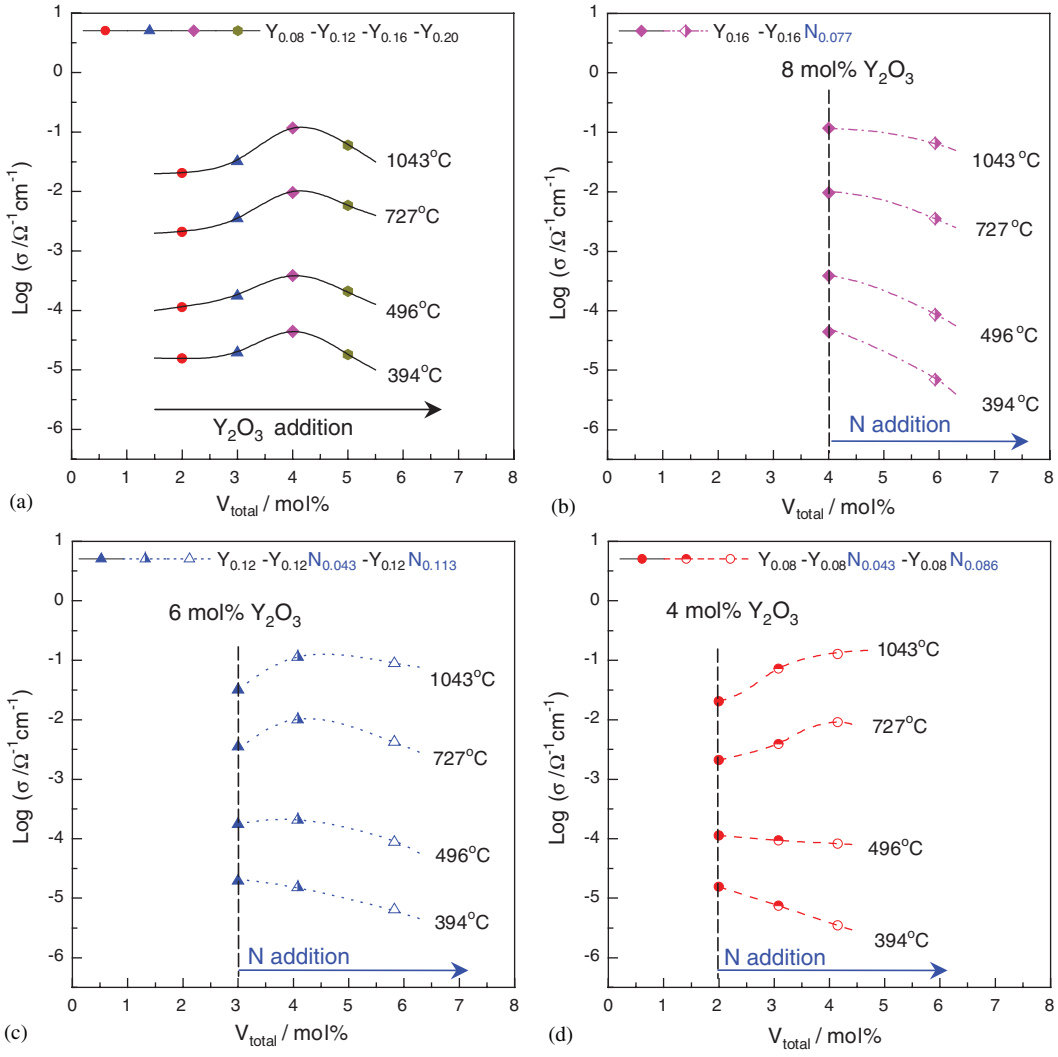

Fig. 5. Conductivity isotherms of zirconia doped with yttria only (a), the isotherms showing the effect of nitrogen addition in the specimen containing 8 mol% Y_2O_3 (b), 6 mol% Y_2O_3 (c), and 4 mol% Y_2O_3 (d), respectively.

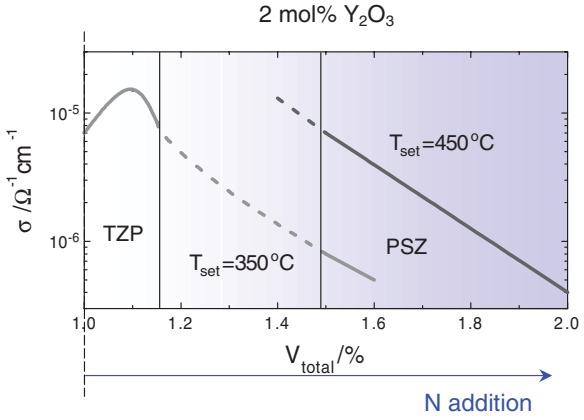

Fig. 6. Conductivity profiles in nitrogen-graded zirconia represented as a function of vacancy concentrations using the nitrogen concentration profiles determined by auger electron spectroscopy.

defect interactions immobilizing oxygen ions, the poor conductivities for low dopant concentrations were ascribed to the presence of monoclinic phase (*m*) [42].

Fig. 8(b) schematically displays the behavior of the $Y_2O_3-ZrO_2$ system, our experimental results of which are shown in the previous section. A qualitative difference from the behavior of $CaO-ZrO_2$ system should be noted here. The maximum at ~8 mol% Y_2O_3 (8YSZ), which is close to the cubic/tetragonal (*t*) boundary, becomes less pronounced mainly because materials with low dopant concentrations (<8 mol%) exhibit relatively high conductivities at lower temperatures. A constant or even decreasing conductivity with increasing dopant concentration in this range (similar to the effects of N addition shown in Figs. 5(d) and 6) has been observed [49,50]. The difference in the conductivity behaviors between $CaO-ZrO_2$ and $Y_2O_3-ZrO_2$ seems not to be simply attributable to the stronger electrostatic interaction in the former, as often supposed [25,26], but suggests qualitatively different defect interactions, defect structures, and superstructures [23,47,51].

The characteristic conductivity bends in $Y_2O_3-ZrO_2$ have been commonly attributed to the association/

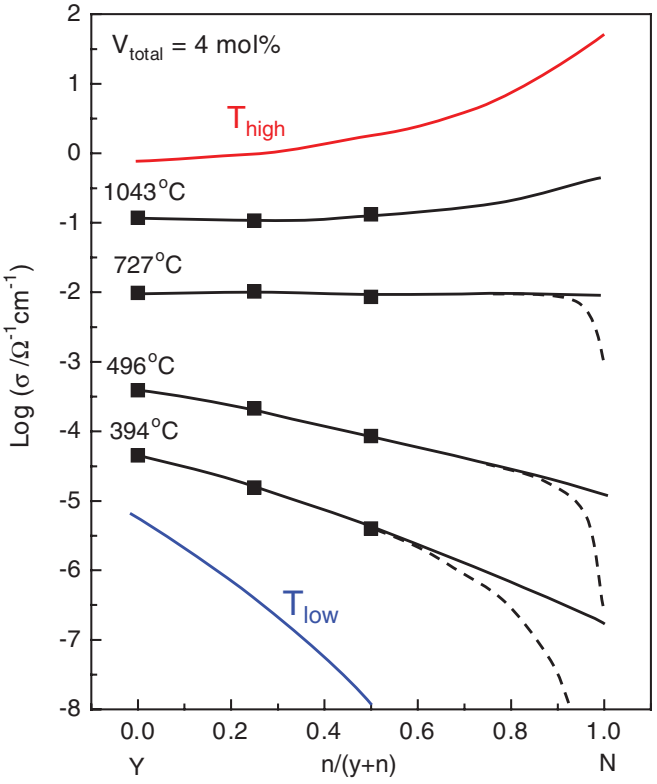

Fig. 7. Square symbols: conductivity isotherms of $Y_yZr_{1-y}O_{2-y/2-3/2n}N_n$ for $(y+n)/4\times100=4$ mol% as a function of the N fraction $(n/(y+n))$. Two isotherms at higher and lower temperature (T_{high}, T_{low}) are schematically indicated. The dashed lines indicate substantial conductivity decrease expected for ordered phase/monoclinic phase in zirconia containing N only.

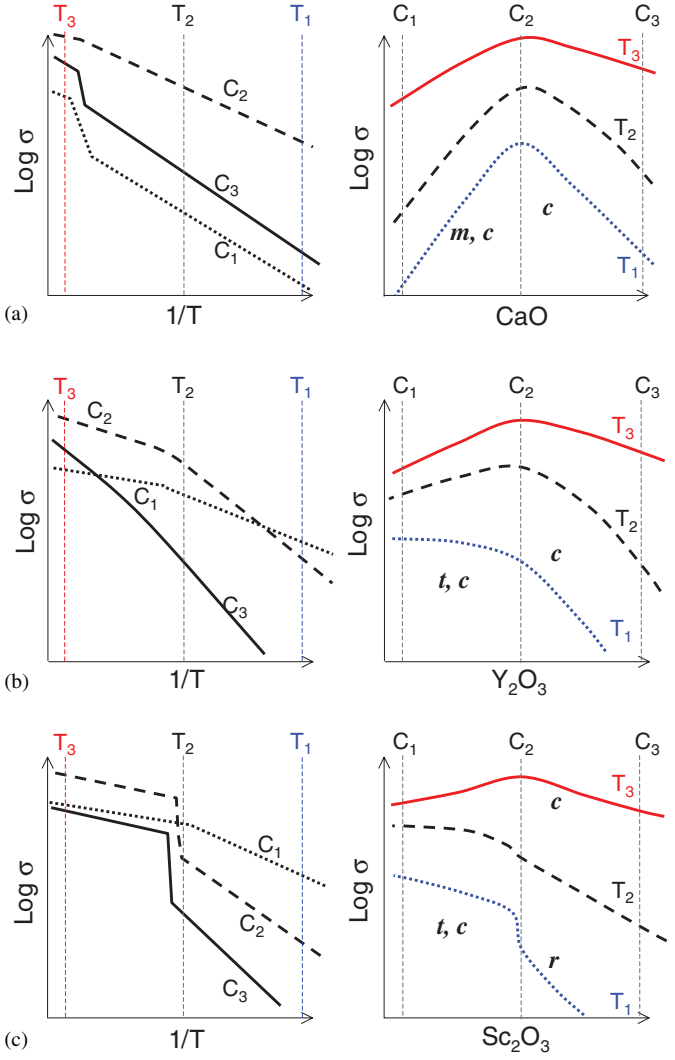

Fig. 8. Conductivity behavior for (a) $CaO-ZrO_2$, (b) $Y_2O_3-ZrO_2$, and (c) $Sc_2O_3-ZrO_2$ system. Left column: schematic temperature dependence of three different dopant compositions in which C_2 is the maximum conductivity composition at high temperatures in the cubic phase region near the tetragonal/cubic phase boundary and C_1 and C_3 are a lower and a higher concentration, respectively. Right column: the isothermal conductivity curves versus dopant concentrations in three different temperatures of T_1, T_2, and T_3.

dissociation of dopant–vacancy complexes. A neutron diffraction study [52] observed the disappearance of the diffuse scattering peaks above the bending temperature and suggested disordering in the micro-domains of correlated vacancy–dopant clusters, rather than breakup of the isolated dopant–vacancy complexes. Another diffraction study showed that the isolated clusters of [1 1 1] vacancy pairs with extensive relaxation fields become mobile at $T>\sim1000$ K [23]. We infer that the phenomena represent an order–disorder transition of vacancy clusters, similarly as in $Sc_2O_3-ZrO_2$ shown in Fig. 8(c) [28,53–56]. The $Sc_2O_3-ZrO_2$ system with a scandia content less than 9 mol%, exhibits conductivity bends around 650 °C, very much like $Y_2O_3-ZrO_2$ system. For high dopant levels (>9 mol%), step-wise transitions accompanied by a cubic–rhombohedral transition occur in $Sc_2O_3-ZrO_2$, while smeared-out transitions are observed in $Y_2O_3-ZrO_2$ (see C_3 curves in Fig. 8(b) and (c)). For the structure of the low-temperature rhombohedral phase observed between 9 and 15 mol% Sc_2O_3, a recent study [57] suggested a [210]-type vacancy correlation. Regardless of the details, however, vacancy-ordered phases are considered to be responsible for the conductivity deterioration in $Sc_2O_3-ZrO_2$ system. It is suggested that the conductivity bends in low Sc_2O_3 compositions as well as those in $Y_2O_3-ZrO_2$ system, all occurring at similar temperatures around 650 °C, should be ascribed to the same nature of interactions, i.e. vacancy-ordering, as for the high dopant levels, rather than introducing a different interaction type of a dopant–vacancy association for the low dopant levels.

Formation of [1 1 1] vacancy pairs and micro-domains of the ordered phase in $Y_2O_3-ZrO_2$ system has been experimentally observed [23,35–37], the energetic preference of which is also supported by theoretical calculations [21,22,30]. Although most of the studies refer to fully stabilized zirconia with $Y_2O_3>9$ mol% [23,35–37,58] the structural characteristics appear to be smoothly extrapolatable to

compositions with lower Y_2O_3 content, in which tetragonally distorted regions with relatively few vacancies increases and the degree of vacancy correlation decreases gradually [48,59,60]. The superior low-temperature conductivity of low Y_2O_3 compositions can thus be ascribed to the lesser clustering of vacancies and probably partly to the high mobility in the tetragonal structure [37,48,58]. Smoothly converging lattice parameters of the tetragonal phase with increasing dopant concentrations [61] are also consistent with the gradual change in defect structure and transport properties across the t/c phase boundary in $Y_2O_3-ZrO_2$ system. Appreciable interaction effects at the dopant levels of ~1 mol% and above are not surprising since they are certainly well above the dilute limit. In fact, no simple correlation between dopant concentrations and the conductivity behavior can be found in the higher dopant range (>4 mol%), which is not unexpected.

The smoother conductivity bends without a macroscopic phase transition in the $Y_2O_3-ZrO_2$ system should be ascribed to the constrained vacancy ordering process. $Zr_3Y_4O_{12}$ is the only known ordered phase in $Y_2O_3-ZrO_2$, which can be obtained only after prolonged annealing [62]. In contrast, $Sc_2O_3-ZrO_2$ exhibits various vacancy-ordered phases [39]. While no cation ordering is found in the ordered $Sc_2O_3-ZrO_2$ phases [57,63], which may be consistent with the negligible dopant–vacancy interaction, the oversized Y ions are preferentially displaced from the nearest-neighbor position to the vacancy due to the repulsive elastic interactions. Thus long-range vacancy ordering around 650 °C is hindered by the distribution of immobile cations in $Y_2O_3-ZrO_2$, while that in $Sc_2O_3-ZrO_2$ occurs irrespective of the cation distribution. It should be noted that the dopants with intermediate ionic radii between Sc and Y, such as Yb and Er, behave intermediately as regards conductivity [27,28,64] and phase characteristics [39,63], suggesting a common interaction mechanism in this series of dopants. In fact, Y appears to be the largest sized dopant exhibiting a pronounced vacancy-ordering interaction. For the larger trivalent dopants such as Gd, Eu, Sm, and Nd, a qualitatively different interaction mode is indicated by the formation of pyrochlore-type ordered phase, $M_2Zr_2O_7$ [39].

Above the vacancy order–disorder transition temperature of ~650 °C, or when the vacancies are randomly distributed, the dopant–vacancy interaction determined by size-mismatch is responsible for the superior conductivity of Sc to Yb and Y, i.e. $\sigma_{Sc} > \sigma_{Yb} > \sigma_Y$ [27,28,64]. At low temperatures, on the other hand, depending on the dopant amount, the conductivity trend can be opposite to that at high temperature, $\sigma_{Sc} < \sigma_{Yb} < \sigma_Y$, as a consequence of the stronger vacancy ordering in the system with the weaker dopant–vacancy interaction. Apparently conflicting co-doping effects in the binary systems of Y–Sc [65–68] or Y–Yb [69,70] can be understood when the two temperature regimes with opposite composition dependencies are considered. Fig. 7 for Y–N binary system then qualitatively describes the Y–Yb and Y–Sc binary systems as well.

The Y–Ca system [26,44,71] may be considered to behave similarly, as Ca substitution was shown to decrease the conductivity below 1000 °C with the tendency becoming stronger with lower temperature, and above 1000 °C a conductivity increase with Ca addition is expected [26]. It should be noted, however, that the total vacancy concentrations vary when the mixtures of 8 mol% $Y_2O_3-ZrO_2$ and 12 mol% $CaO-ZrO_2$ are compared [26]. For compositions with fixed total vacancy concentrations a non-monotonic composition dependence was observed at 350 °C [71]. The behavior appears to be related to the different stabilizing effects and the different types of defect interactions between the two dopants as discussed above. The co-doping effects in Y–Ca–Zr–O system are apparently more involved [44] than in Y–Sc–Zr–O and Y–Yb–Zr–O systems.

In Fig. 7 the dotted curves represents a drastic ionic conductivity decrease expected for zirconia containing N only, since vacancy-ordered phases and monoclinic phase form below 1000 °C. However, as long as a small amount of Y stabilizes the tetragonal and cubic phase with more or less randomly distributed vacancies [1,2,4,5,10,11], a gradual conductivity change is expected. The only available literature data of β-phase $Zr_7O_8N_4$ (conductivity of $5.4 \times 10^{-10}\,\Omega^{-1}\,cm^{-1}$ at 400 °C and activation energy of 1.77 eV) [72] points towards strong interactions in the ordered phase of N-containing zirconia. (Ref. [72] suggested that the material is semiconducting, which seems to be further clarified.) Interestingly, a similar behavior has been recently reported for the Y–Sc system [67]: while zirconia with 11 mol% Sc_2O_3 exhibits a very low conductivity due to the formation of vacancy-ordered rhombohedral phases, substitution of only 1 mol% Y_2O_3 stabilizes zirconia in the cubic phase and thus results in a substantially enhanced conductivity.

5. Conclusion

The comparison of conductivity behaviors of zirconia doped with nitrogen and conventional cation stabilizers leads to the following conclusion: for N-doped zirconia as well as zirconia with size-matched cation stabilizers, such as Sc, Yb and Y, the elastically driven vacancy–vacancy ordering interaction phenomenologically accounts for the temperature- and composition-dependence. It is emphasized that for the dopant range in which high-temperature conductivity may still increase with dopant concentration, at low temperatures below the vacancy order–disorder transition, the conductivity deteriorates with dopant concentration due to strong defect interactions. It is also shown that materials with size-matched dopants exhibit superior high-temperature conductivity due to weak dopant–vacancy interactions, but, as the vacancy ordering process is consequently favorable as well, undergo a pronounced conductivity deterioration at low tempera-

tures. The analysis explains the qualitatively similar mixed-dopant effects in Y–Yb and Y–Sc-co-doped system as well as in Y–N system. The addition of a small amount of Y in N-doped zirconia or in Sc-doped zirconia can hinder the formation of long-range ordered phases and thus enhance the conductivity substantially.

References

[1] Y.-B. Cheng, D.P. Thompson, J. Am. Ceram. Soc. 74 (1991) 1135.
[2] Y.-B. Cheng, D.P. Thompson, J. Am. Ceram. Soc. 76 (1993) 683.
[3] M. Lerch, J. Am. Ceram. Soc. 79 (1996) 2641.
[4] T.-J. Chung, J.-S. Lee, H. Song, D.-Y. Kim, J. Am. Ceram. Soc. 82 (1999) 3193.
[5] T.-J. Chung, J.-S. Lee, G.-H. Kim, H. Song, D.-Y. Kim, J. Am. Ceram. Soc. 84 (2001) 172.
[6] J.C. Gilles, Bull. Soc. Chim. France 22 (1962) 2118.
[7] R. Collongues, J.C. Gilles, A.M. Lejus, M.P.Y. Jorba, D. Michel, Mater. Res. Bull. 2 (1967) 837.
[8] N. Claussen, R. Wagner, L.J. Gauckler, G. Petzow, J. Am. Ceram. Soc. 61 (1978) 369.
[9] G.V. Tendeloo, G. Thomas, Acta Metall. 31 (1983) 1611.
[10] M. Lerch, J. Wrba, J. Lerch, J. Solid State Chem. 125 (1996) 153.
[11] J. Wrba, M. Lerch, J. Eur. Ceram. Soc. 18 (1998) 1787.
[12] M. Lerch, O. Rahäuser, J. Mater. Sci. 32 (1997) 1357.
[13] A.T. Tham, C. Rödel, M. Lerch, D. Wang, D.S. Su, A. Klein-Hoffmann, R. Schlögl, Cryst. Res. Technol. 40 (2005) 193.
[14] M. Kilo, M.A. Taylor, C. Argirusis, G. Borchardt, M. Lerch, O. Kaitasov, B. Lesage, Phys. Chem. Chem. Phys. 6 (2004) 3645.
[15] I. Kaiser-Bischoff, H. Boysen, F. Frey, J.-U. Hoffmann, D. Hohlwein, M. Lerch, J. Appl. Crystallogr. 38 (2005) 139.
[16] I. Kaiser-Bischoff, H. Boysen, F. Frey, C. Sherf, T. Hansen, Phys. Chem. Chem. Phys. 7 (2005) 2061.
[17] J.-S. Lee, T.-J. Chung, D.-Y. Kim, Solid State Ionics 136–137 (2000) 39.
[18] J. Wendel, M. Lerch, W. Laqua, J. Solid State Chem. 142 (1999) 163.
[19] J.-S. Lee, J. Fleig, J. Maier, T.-J. Chung, D.-Y. Kim, J. Am. Ceram. Soc. 88 (2005) 3067.
[20] M.O. Zacate, L. Minervin, D.J. Bradfield, R.W. Grimes, K.E. Sickafus, Solid State Ionics 128 (2000) 243.
[21] A. Bogicevic, C. Wolverton, G.M. Crosbie, E.B. Stechel, Phys. Rev. B 64 (2001) 014106.
[22] A. Bogicevic, C. Wolverton, Phys. Rev. B 67 (2003) 024106.
[23] J.P. Goff, W. Hayes, S. Hull, M.T. Hutchings, K.N. Clausen, Phys. Rev. B 59 (1999) 14202.
[24] A. Bogicevic, C. Wolverton, Europhys. Lett. 56 (2001) 393.
[25] T.H. Etcell, S.N. Flengas, Chem. Rev. 70 (1970) 339.
[26] J. Gong, Y. Li, Z. Zhang, Z. Tang, J. Am. Ceram. Soc. 83 (2000) 648.
[27] J.A. Kilner, R.J. Brook, Solid State Ionics 6 (1982) 237.
[28] Y. Arachi, H. Sakai, O. Yamamoto, Y. Takeda, N. Imanishai, Solid State Ionics 121 (1999) 133.
[29] G. Stapper, M. Bernasconi, N. Nicoloso, M. Parrinello, Phys. Rev. B 59 (1999) 797.
[30] S. Fabris, A.T. Paxton, M.W. Finnis, Acta Mater. 50 (2002) 5171.
[31] C.R.A. Catlow, A.V. Chadwick, G.N. Greaves, L.N. Moroney, J. Am. Ceram. Soc. 69 (1986) 272.
[32] P. Li, I.W. Chen, J.E. Pennerhahn, Phys. Rev. B 48 (1993) 10074.
[33] J.G. Allpress, H.J. Rossell, J. Solid State Chem. 15 (1975) 68.
[34] T. Proffen, R.B. Neder, F. Frey, Acta Crystallogr. B 52 (1996) 59.
[35] D.N. Argyriou, M.M. Elcombe, A.C. Larson, J. Phys. Chem. Solids 57 (1996) 183.
[36] D. Steele, B.E.F. Fender, J. Phys. C: Solid State Phys. 7 (1974) 1.
[37] N.H. Andersen, K. Clausen, M.A. Hackett, W. Hayes, M.T. Hutchings, J.E. Macdonald, R. Osborn, Physica B 136 (1986) 315.
[38] A.T. Tham, C. Rödel, M. Lerch, D. Wang, D.S. Su, A. Klein-Hoffmann, R. Schlögl, Cryst. Res. Technol. 39 (2004) 421.
[39] H. Ondik, H. McMurdie (Eds.), Phase Diagrams for Zirconium and Zirconia Systems, American Ceramic Society, Westerville, OH, 1998.
[40] M. Lerch, F. Krumeich, R. Hock, Solid State Ionics 95 (1997) 87.
[41] M. Lerch, H. Boysen, P. Radaelli, J. Phys. Chem. Solids 58 (1997) 1557.
[42] T.Y. Tien, E.C. Subbarao, J. Chem. Phys. 39 (1963) 1041.
[43] T.Y. Tien, J. Am. Ceram. Soc. 47 (1964) 430.
[44] D.W. Strickler, W.G. Carlson, J. Am. Ceram. Soc. 47 (1964) 122.
[45] S.H. Chu, M.A. Seitz, J. Solid State Chem. 23 (1978) 297.
[46] R.E. Carter, W.L. Roth, in: C.B. Alcock (Ed.), Electromotive Force Measurements in High Temperature Systems, I.M.M. London, 1968, pp. 125–132.
[47] T. Proffen, R.B. Neder, F. Frey, D.A. Keen, C.M.E. Zeyen, Acta Crystallogr. B 49 (1993) 605.
[48] U. Martin, H. Boysen, F. Frey, Acta Crystallogr. B 49 (1993) 403.
[49] S.P.S. Badwal, Solid State Ionics 52 (1992) 23.
[50] X. Guo, J. Maier, J. Electrochem. Soc. 148 (2001) E121.
[51] H.J. Rossell, in: A.H. Heuer, L.W. Hobbs (Eds.), Science and Technology of Zirconia, American Ceramic Society, Westerville, OH, 1981, pp. 47–63.
[52] I.R. Gibson, J.T.S. Irvine, J. Mater. Chem. 6 (1996) 895.
[53] F.M. Spiridonov, L.N. Popova, R.Y. Popil'skii, J. Solid State Chem. 2 (1970) 430.
[54] S.P.S. Badwal, J. Mater. Sci. 18 (1983) 3117.
[55] S.P.S. Badwal, J. Mater. Sci. 22 (1987) 4125.
[56] S.P.S. Badwal, F.T. Ciacchi, D. Milosevic, Solid State Ionics 136–137 (2000) 91.
[57] K. Wurst, E. Schweda, D.J.M. Bevan, J. Mohyla, K.S. Wallwork, M. Hofmann, Solid State Sci. 5 (2003) 1491.
[58] S. Hull, T.W.D. Farley, M.A. Hackett, W. Hayes, R. Osborn, N.H. Andersen, K. Clausen, M.T. Hutchings, W.G. Stirling, Solid State Ionics 28–30 (1988) 488.
[59] C.J. Howard, R.J. Hill, B.E. Reichert, Acta Crystallogr. B 44 (1988) 116.
[60] D.N. Argyriou, C.J. Howard, J. Appl. Crystallogr. 3 28 (1995) 206.
[61] H.G. Scott, J. Mater. Sci. 10 (1975) 1527.
[62] V.S. Stubican, R.C. Hink, S.P. Ray, J. Am. Ceram. Soc. 61 (1978) 17.
[63] H.J. Rossell, J. Solid State Chem. 19 (1976) 103.
[64] D.W. Strickler, W.G. Carlson, J. Am. Ceram. Soc. 48 (1965) 286.
[65] H. Kaneko, F. Jin, H. Taimatsu, J. Am. Ceram. Soc. 76 (1993) 793.
[66] F.T. Ciacchi, S.P.S. Badwal, J. Eur. Ceram. Soc. 7 (1991) 197.
[67] T.I. Politova, J.T.S. Irvine, Solid State Ionics 168 (2004) 153.
[68] S.P.S. Badwal, F.T. Ciacchi, S. Rajendran, J. Drennan, Solid State Ionics 109 (1998) 167.
[69] G.S. Corman, V.S. Stubican, J. Am. Ceram. Soc. 68 (1985) 174.
[70] Y. Li, J. Gong, Y. Xie, Z. Tang, Z. Zhang, Mater. Sci. Eng. B 90 (2002) 287.
[71] M.M. Bućko, J. Eur. Ceram. Soc. 24 (2004) 1305.
[72] M. Ohashi, H. Yamamoto, S. Yamanaka, M. Hattori, Mater. Res. Bull. 28 (1993) 513.